Proc. Natl. Acad. Sci. USA
Vol. 83, pp. 8152–8156, November 1986
Biophysics

Isotope effect on electron transfer in reaction centers from *Rhodopseudomonas sphaeroides*

(bacterial photosynthesis/vibronic coupling/hydrogen bonding/kinetics)

M. Y. Okamura and G. Feher

Department of Physics, University of California, San Diego, La Jolla, CA 92093

Contributed by G. Feher, July 2, 1986

ABSTRACT **Previous ENDOR studies on reaction centers from *Rhodopseudomonas sphaeroides* have shown the presence of two hydrogen-bonded protons associated with the primary, ubiquinone, acceptor Q_A. These protons exchange with deuterons from solvent ^2H_2O. The effect of this deuterium substitution on the charge-recombination kinetics $(BChl)_2^+Q_A^- \rightarrow (BChl)_2Q_A$ has been studied with a sensitive kinetic difference technique. The electron-transfer rate was found to increase with deuterium exchange up to a maximum $\Delta k/k$ of 5.7 ± 0.3%. The change in rate was found to have an exchange time of 2 hr, which matched the disappearance of the ENDOR lines due to the exchangeable protons. These results indicate that these protons play a role in the vibronic coupling associated with electron transfer. A simple model for the isotope effect on electron transfer predicts a maximum rate increase of 20%, which is consistent with the experimental results.**

The primary photochemistry in bacterial photosynthesis involves light-induced electron transfer in a bacteriochlorophyll (BChl) protein complex called the reaction center (RC) (for reviews, see refs. 1–3). The absorbed photon excites a primary donor species, a BChl dimer, which transfers an electron to a bacteriopheophytin (BPh) molecule. Subsequent electron transfer occurs from BPh to a primary quinone, Q_A, and then to a secondary quinone, Q_B.

The structural basis for electron transfer in bacterial RCs has been investigated by a wide variety of biochemical and biophysical techniques, including the recent x-ray crystallographic structure determination by Deisenhofer *et al.* (4, 5) of the RC from *Rhodopseudomonas viridis*. The structure of the *Rhodopseudomonas sphaeroides* RC used in this study is assumed to be very similar to that of *R. viridis*. This assumption is based on the amino acid sequence homology between the two RCs (6–8) and the preliminary electron density mapping of the RC from *R. sphaeroides* by the molecular replacement method (9). The components of the electron-transfer chain (BChl dimer, BPh, and Q_A) are arranged in series across the membrane. The secondary quinone, Q_B, is related to Q_A by an approximately 2-fold symmetry axis. An Fe^{2+} coordinated to four histidine residues is located between the two quinones.

The success of the structural studies of bacterial RCs has motivated us to investigate the structural basis for the electron-transfer reactions. Theories of electron transfer require the coupling of electron transfer to vibrational motion (intermolecular or intramolecular) of the molecules involved in the reaction (10–14). This coupling is necessary to match the energies of the product and reactant state (i.e., to form the transition state for electron transfer). The coupling enables the excess energy of the reactant state to be given off to the lattice. The goal of this study was to identify the vibrational modes that play a role in the electron transfer. The approach that was adopted is based on the effect of isotope substitution on the rate of electron transfer.

Recent ENDOR studies (15, 16) on *R. sphaeroides* RCs in which Fe^{2+} has been replaced by the diamagnetic Zn^{2+} (17) have shown the presence of two protons magnetically coupled to Q_A^-. These protons exchange with deuterons from solvent ^2H_2O (D_2O) with an exchange time of several hours. They have been tentatively assigned to two protons hydrogen-bonded to Q_A (15, 16). In this study we investigate the effect of substituting deuterium for these exchangeable protons on the rate of the electron-transfer reaction

$$(BChl)_2^+Q_A^- \xrightarrow{k} (BChl)_2Q_A. \qquad [1]$$

This reaction has been extensively studied by a variety of approaches (see refs. 18–20 for reviews). Its rate is approximately temperature independent (activationless) down to cryogenic temperatures (21–25). This behavior has been explained by postulating that the potential-energy surface of the product state intersects the energy surface of the reactant state near its energy minimum (26, 27). This model is used to explain the isotope effect observed for the above electron-transfer reaction (Eq. 1). A preliminary report of this work has been presented (28).

MATERIALS AND METHODS

Sample Preparation. RCs were prepared as described (29). The quinone content was adjusted to approximately one quinone per RC by treatment with 1% lauryldimethylamine oxide and *o*-phenanthroline (30). The final step was dialysis against 0.025% lauryldimethylamine oxide followed by concentration in a Centricon filtration cell. The RCs were then diluted (typically 1:19) into either D_2O buffer or H_2O buffer (pH 8.0) containing 0.025% sodium cholate. The pH of the D_2O buffer was measured to be 8.0 using an electrode standardized in H_2O.

Kinetic Measurements. The kinetic measurements were made on a spectrometer described earlier (31). The absorbance changes produced by a laser flash were monitored at 865 nm (or at 890 nm at low temperature). Unless otherwise specified, the temperature of the sample was held at 20.0 ± 0.2°C. The first measurement was made after 5 min of incubation. We define this as the $t = 0$ time point. Typically, the transients from 10 flashes were averaged, converted to absorbance, and normalized to a maximum absorbance change of −1.00. Kinetic difference traces were obtained by subtracting the normalized trace taken at $t = 0$ from the normalized traces taken after different incubation times. The change in rate was obtained from the difference traces by using the relations derived from the following analysis.

The publication costs of this article were defrayed in part by page charge payment. This article must therefore be hereby marked "*advertisement*" in accordance with 18 U.S.C. §1734 solely to indicate this fact.

Abbreviations: RC, reaction center; BChl, bacteriochlorophyll; BPh, bacteriopheophytin; t_{inc}, incubation time in ^2H_2O; t_{exch}, exchange time.

Analysis of Data. For a deuterium exchange experiment in which the RC contains either hydrogen or deuterium bound to a site that influences the electron transfer, the normalized absorbance as a function of time after a laser flash can be expressed as:

$$A(t) = A_0(\alpha e^{-k_D t} + (1 - \alpha)e^{-k_H t}), \quad [2]$$

where α, the fraction of RCs containing deuterium, depends on the incubation time in D_2O, t_{inc}. The rate constants k_D and k_H refer to the deuterated and protonated species, respectively. A_0 is a normalization constant ($A_0 = -1.0$). The difference $\Delta A(t)$ between the normalized absorbance traces taken after an incubation time t_{inc} and the trace taken at $t_{inc} = 0$ is obtained by subtracting the decay due to the protonated species alone, $A_0e^{-k_H t}$, from Eq. 2. The result for small changes in rate, $k_D - k_H = \Delta k << k_H$, is given by:

$$\Delta A(t) = \alpha A_0 e^{-k_H t}(\Delta k t). \quad [3]$$

This function is zero at $t = 0$ and $t = \infty$ and has a maximum at $t = 1/k$. The maximum value of this function is

$$\Delta A_M(t_{inc}) = -\frac{\alpha A_0 \Delta k}{ek}, \quad [4]$$

which is proportional to α and, thus, is a measure of the extent of deuterium exchange. From Eq. 4 at long exchange times ($t_{inc} = \infty$, $\alpha = 1$), the maximum value of ΔA_M is related to the change in rate by:

$$\frac{\Delta k}{k} = -e\frac{\Delta A_M(\max)}{A_0}. \quad [5]$$

Comparison of Kinetic Changes with ENDOR Amplitudes. To correlate the time course of the effects of deuterium exchange on the ENDOR spectrum and the optical decay kinetics, the two types of measurements were made on the same samples. In these samples Zn^{2+} was substituted for Fe^{2+} (17) and deuterated ubiquinone was substituted for the native ubiquinone (30) to simplify the ENDOR spectrum, thereby facilitating the quantitation of the exchangeable protons. After dilution into D_2O, the optical kinetics and ENDOR spectra were measured after different incubation times. The ENDOR samples were reduced with 50 mM Na dithionite and analyzed at 115 K in a spectrometer of local design (15, 16). The amplitudes of the peaks due to the exchangeable protons were normalized to the matrix ENDOR peak near the proton Larmour frequency.

RESULTS

The change in the electron-transfer rate upon deuteration of the RCs was measured by monitoring the recovery of the flash-induced optical absorption transient at 865 nm after different incubation (exchange) times. The results obtained on a sample that was incubated in D_2O for 0 and 3.5 hr show a small rate increase with incubation in D_2O (see Fig. 1*a*). To measure the small changes more conveniently, the two normalized traces were subtracted from each other. The resultant difference trace is shown in Fig. 1*b*. Its shape is described by Eq. 3; the peak ΔA_M appears at $t = 1/k = 120$ ms, which is the recombination time between Q_A^- and $(BChl)_2^+$.

RCs diluted into H_2O buffer did not show an increase in ΔA_M (see the lower trace of Fig. 1*b*). Instead a small decrease was sometimes observed. RCs diluted into H_2O buffered at a different pH (pH 7 or 9) showed negligible changes in rate between 5 min and 3 hr of incubation, indicating that the

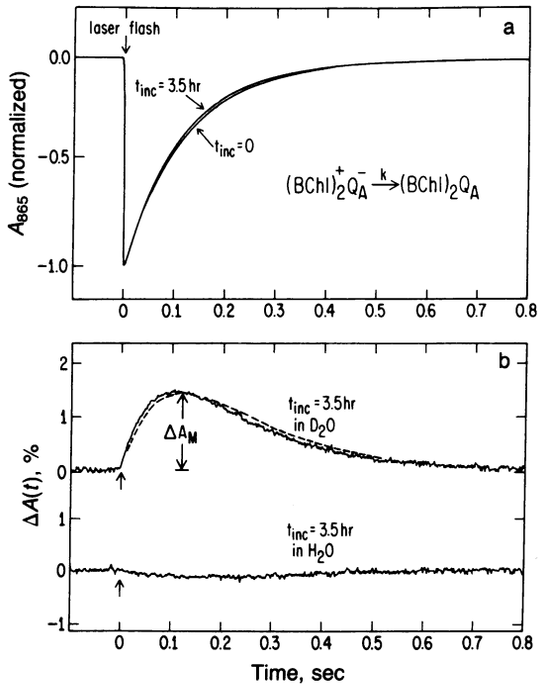

FIG. 1. (*a*) Electron-transfer kinetics monitored by flash-induced optical absorbance changes (λ = 865 nm) in RCs (5 μM in 10 mM Tris chloride, pH 8.0/0.025% cholate at 20°C) after incubation in D_2O. Each trace is normalized to a maximum change of −1.00 and represents the average of 10 traces. Note the increase in rate upon deuteration. (*b*) Kinetic difference traces. The normalized traces taken at $t_{inc} = 0$ were subtracted from the traces taken at 3.5 hr. The scale is given in terms of the percent of the maximum absorption change. The sample incubated in D_2O shows a peak ΔA_M in the difference trace due to a change in rate. This peak is absent in the control sample incubated in H_2O. The dashed line is a fit to the equation $\Delta A_M e^{(1-kt)}kt$ (obtained from Eqs. 3 and 4) for $1/k$ = 120 ms.

change observed in D_2O is not due to the change in the ionization of charged groups on the protein (data not shown). Differences in rate between RCs diluted into D_2O and H_2O measured after short (5 min) incubation times were observed. [ΔA_M ($D_2O - H_2O$) ≈ −0.5%; i.e., $\Delta k/k \approx -1.4\%$]. This small decrease in rate is due to effects that occur rapidly upon dilution into D_2O.

To determine the changes in rate due to slowly exchanging protons, $\Delta A_M(t_{inc})$ was measured after different incubation times subsequent to an initial 5-min incubation period. The results in Fig. 2*a* are characteristic of a single exponential deuterium exchange process with an exchange rate = $1/t_{exch}$, where t_{exch} is the exchange time. The solid line represents a fit to the function

$$\Delta A_M(t_{inc}) = \Delta A_M(\max)[1 - e^{-t_{inc}/t_{exch}}], \quad [6]$$

from which the values of $\Delta A_M(\max)$ and t_{exch} were obtained. The results of five experiments gave values for $\Delta A_M(\max)$ = 2.1 ± 0.1% and t_{exch} = 2.0 ± 0.2 hr. The maximum value for ΔA_M corresponds to an increase in the rate due to deuterium substitution (from Eq. 5) of

$$\Delta k/k = 5.7 \pm 0.3\%. \quad [7]$$

Experiments with other buffers (containing 0.025% lauryldimethylamine oxide or 50 μM terbutryn) gave similar results (data not shown).

The reverse exchange reaction (i.e., the substitution of hydrogen for deuterium) was measured by first incubating RC in D_2O buffer for 1 day. The deuterated RCs were then diluted

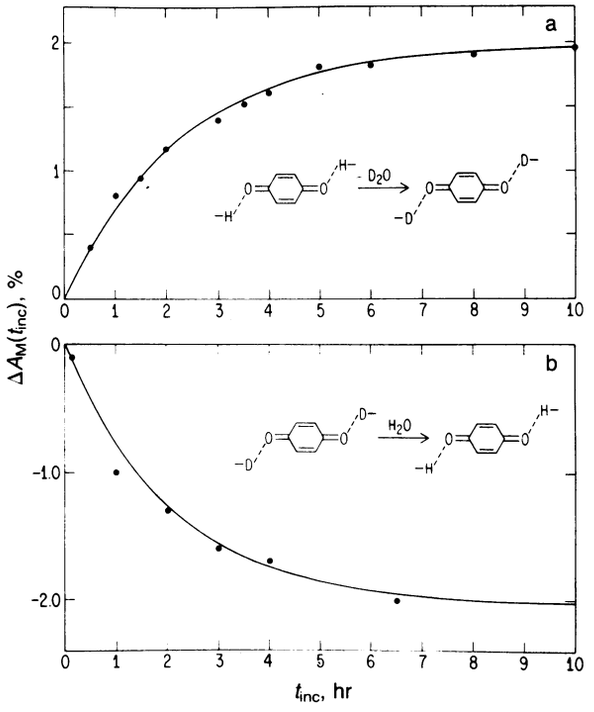

FIG. 2. (*a*) Dependence of ΔA_M on incubation time, t_{inc}. The ΔA_M is corrected for changes due to dilution in H_2O. The solid line is a fit to Eq. **6** for $\Delta A_M(max) = -2.0\%$ and $t_{exch} = 2.3$ hr. (*b*) The dependence of ΔA_M for deuterated RCs diluted into H_2O. The solid line is a fit to Eq. **6** for $\Delta A_M(max) = -2.05\%$, $t_{exch} = 2.1$ hr. The reversed sign of ΔA_M is expected for a reversible isotope effect.

into H_2O buffer, and the change in rate was measured. Fig. 2*b* shows that the electron-transfer reaction slowed down (ΔA_M is negative) as expected for the reversal of the deuterium substitution. The values obtained were $\Delta A_M = -2.05\%$ and $t_{exch} = 2.1$ hr, essentially the same as found for the proton-to-deuteron exchange.

To assign the isotope effect to the exchangeable protons on Q_A previously observed in ENDOR experiments (15, 16), we need to demonstrate that t_{exch} determined from the amplitudes of the ENDOR lines is the same as that obtained from the kinetic studies. Fig. 3 shows the two low-frequency

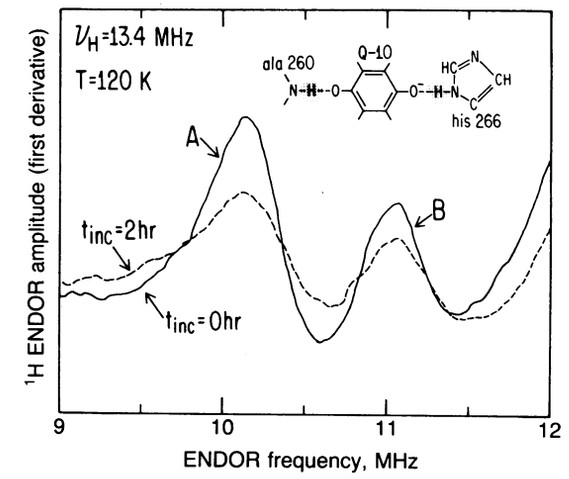

FIG. 3. ENDOR spectra of the exchangeable protons in RCs incubated in D_2O for 0 hr (solid line) and 2 hr (dashed line). The samples (50 μl, 70 μM RC) were reduced with sodium dithionite, frozen, and run at 120 K. Traces were averaged for 10 hr and normalized to the peak in the matrix region.

ENDOR peaks at 3.2 and 2.3 MHz below the proton Larmour frequency of 13.4 MHz. These correspond to hyperfine couplings of 6.4 and 4.7 MHz associated with the two exchangeable protons on Q_A (15, 16). The two traces shown in Fig. 3 correspond to incubation times of $t_{inc} = 0$ hr and $t_{inc} = 2.0$ hr. The amplitudes of both peaks were considerably reduced after 2 hr of incubation in D_2O.

The exchange times for the exchangeable protons were measured from the change in the ENDOR amplitudes. A comparison between the change in amplitudes of the two ENDOR lines and the change in rate due to deuterium substitution by kinetic measurements is shown in Fig. 4. The best fit of the data for the two ENDOR peaks was obtained with $t_{exch} = 2.0 \pm 0.2$ hr and 2.2 ± 0.2 hr for peaks A and B, respectively, and for the optical decay kinetics with $t_{exch} = 1.9 \pm 0.2$ hr. These times are the same within experimental error, leading to the conclusion that the isotope effect is due to the exchangeable protons.

The effect of isotope substitution on the low-temperature electron-transfer kinetics was studied by incubating RCs for various times in D_2O at 20°C and then freezing them in 50% (deuterated) glycerol. The kinetics were measured at 80 K. The fractional change in the low-temperature rate [$\Delta A_M(max) = 2.0 \pm 0.2\%$, $\Delta k/k = 5.4 \pm 0.5\%$] was very similar to the change seen at room temperature, even though the absolute rate at low temperature was faster by about a factor of 4 ($1/k = 27$ ms).

DISCUSSION

Although the sequence of electron-transfer reactions and the structure of the electron-transfer components in the bacterial RC is now well established, the mechanism of electron transfer in the RC is not fully understood. In this work we examined the effect of deuterating exchangeable protons on the rate of electron transfer between Q_A^- and $(BChl)_2^+$. We find that deuteration of the RC by incubation in D_2O increases the rate of this electron-transfer reaction by ≈6%. The time course for the rate increase matches the time course for the exchange of the H-bonded protons associated with Q_A as determined by ENDOR experiments. Therefore, we assign the rate increase to these protons. Although many protons are exchanged for deuterons by incubation of the RC in D_2O, our method of measurement discriminates against changes that occur rapidly—e.g., those due to rapidly exchangeable protons, changes in the pK_a of ionizable groups, or changes in viscosity.

The structural assignment of these ENDOR peaks to protons on the RC can be tentatively made on the basis of the

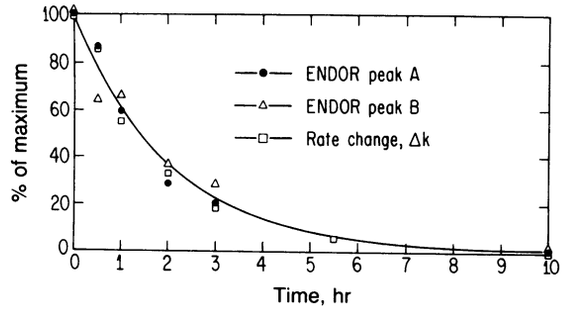

FIG. 4. Comparison between the time course for the loss of the ENDOR spectra of the exchangeable protons and the change in the electron-transfer rate. The normalized ENDOR data points were obtained by subtracting from the measured (see Fig. 3) peak-to-peak amplitudes, the amplitudes that were obtained from a sample that was incubated for 10 hr in D_2O. The rate changes were plotted as $100[1 - \Delta A_M(t_{inc})/\Delta A_M(max)]$ for comparison. The solid line is the function $100\, e^{-t_{inc}/t_{exch}}$ for $t_{exch} = 2.0$ hr.

x-ray crystal structure of *R. viridis* (5). One of the protons is assigned a peptide NH-group hydrogen-bonded to Q_A (Ala-258 and Ala-260 in *R. viridis* and *R. sphaeroides*, respectively). The second hydrogen bond is assigned to an imidazole NH group of one of the Fe-coordinated histidines that is near the carbonyl group of Q_A. (His-264 and His-266 in *R. viridis* and *R. sphaeroides*, respectively) (see Fig. 3 *Inset*).

We shall next try to explain the observed isotope effect in terms of theories of electron transfer (10–14, 26, 27). Current theories express the transfer rate in terms of a matrix element $V(r)$ and a Franck–Condon factor $F(\Delta x_i)$:

$$k \propto |V(r)|^2 F(\Delta x_i). \quad [8]$$

$V(r)$ is due to the overlap of the electronic donor and acceptor wavefunctions and depends on the donor–acceptor distance r. To a first approximation, $V(r)$ should be independent of the mass of the reacting species. $F(\Delta x_i)$ describes the coupling of the fluctuations in internuclear distances Δx_i for various vibrational modes of the system to the electronic energy for the reactants and products; this coupling depends on the temperature and nuclear masses. Thus, the isotope effect is expected to arise predominantly from changes in $F(\Delta x_i)$.

The magnitude of the isotope effect depends on the details of the vibrational coupling mechanism. Different functional forms of the $F(\Delta x_i)$ have been described by different workers (10–14, 26, 27). We shall examine the theoretical prediction for the simple limiting case of a single high-frequency vibrational mode with frequency ω at low temperature, with the additional assumption that the difference in redox energy ΔE_{redox} is equal to the reorganization energy E_r (26, 27). For this (activationless) case, the electron transfer occurs from the ground vibrational state with a rate that is predicted to be nearly temperature independent, as is found experimentally to be the case for the charge recombination between Q_A^- and $(BChl)_2^+$ (21–25). The isotope effect for this case can be estimated by an extension of the classical theory of electron transfer (10) to low temperature by semiclassical (11) or detailed quantum mechanical (12) treatments. For the case of localized modes at low temperature, both treatments lead to the same result. A simplified physical description of this result is described below.

The reaction is considered to occur from the ground vibrational quantum level of the reactant state. Since the electron transfer occurs to excited vibrational levels, the product state is treated classically as a continuum (see Fig. 5*a*). Electron transfer occurs in a region near the intersection of the product and reactant potential energy curves (the transition state). The width of this intersection region depends on the matrix element $|V(r)|^2$ and is independent of isotopic substitution. The reaction rate is proportional to the probability of being in the intersection region. If the intersection is near the minimum of the reactant state, this probability is inversely proportional to δx_0, where δx_0 is the width of the probability distribution of the ground state due to zero point motion along the reaction coordinate (see Fig. 5*a*). For a harmonic oscillator, the width, δx_0, is proportional to the square root of the vibrational frequency. Since ω is inversely proportional to the square root of the reduced mass, μ, [$\omega = (\kappa/\mu)^{1/2}$], the width δx_0 is inversely proportional to $\mu^{1/4}$, and hence the probability density and electron-transfer rate are proportional to $\mu^{1/4}$. The physical interpretation of this is that the RC containing the heavier isotope reacts faster because there is a higher probability density at the transition state. If the vibrational coupling were totally due to vibrations in the hydrogen bond, this would lead to an increase in rate given by

$$\frac{k_D}{k_H} = \left[\frac{(\mu_D)}{(\mu_H)}\right]^{1/4} \simeq [2]^{1/4} \simeq 1.2. \quad [9]$$

The observed result $k_D/k_H = 1.06$ is in the right direction and is of the right order of magnitude. The difference between the measured isotope effect and the result predicted by Eq. 9 probably indicates that the simplifying assumptions made in this model may not be correct—i.e., (*i*) the vibronic coupling to electron transfer may be more complex (e.g., more than one vibrational mode may contribute to electron transfer), (*ii*) the values for ΔE_{redox} and the reorganization energy may not exactly match, and (*iii*) the reaction may not be in the low-temperature limit. All of these conditions would lead to a lower value for k_D/k_H. Thus, the predicted result should be considered an upper limit for the isotope effect.

Kihara and McCray (32) have found a deuterium isotope effect for the electron-transfer reaction from cytochrome *c* to

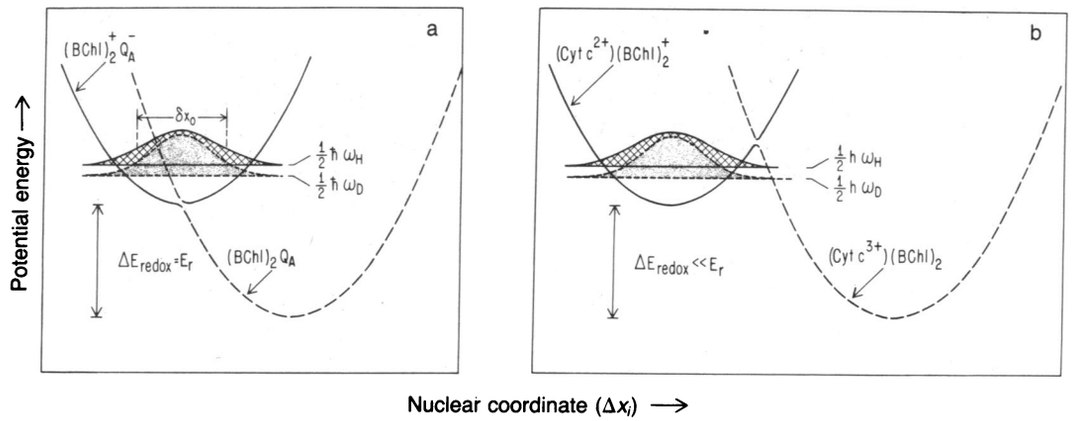

FIG. 5. The potential energy vs. nuclear coordinate shown for two cases of electron-transfer reactions that exhibit deuterium isotope effects: the temperature-independent (activationless) case (*a*)—e.g., $(BChl)_2^+Q_A^- \rightarrow (BChl)_2Q_A$—and the temperature-dependent (activated) case (*b*)—e.g., Cyt $c^{2+}(BChl)_2^+ \rightarrow$ Cyt $c^{3+}(BChl)_2$. The nuclear coordinate is the length of a hydrogen bond. The reaction in this (low temperature) approximation occurs from the ground vibrational state of the reactant manifold (the solid parabolas). The probability density distribution for the ground vibrational state is shown for the protonated species ($E = 1/2\hbar\omega_H$, solid curve) and the deuterated species ($E = 1/2\hbar\omega_D$, dashed curve). Deuteration increases the probability density in the center of the distribution and decreases it in the wings. Since the reaction rate is proportional to the probability density at the transition state (i.e., the crossing point between the potential energy curves of the two parabolas), this simple model predicts an increase in electron transfer on deuteration for the temperature-independent reaction (*a*), in which the crossing occurs near the peak of the distribution, and a decrease in the electron-transfer rate on deuteration for the temperature-dependent case (*b*), in which the crossing occurs in the wings of the distribution.

D^+. The onset of their isotope effect occurred immediately upon addition of D_2O and must be due to rapidly exchangeable protons. The magnitude of the isotope effect reported for the electron transfer from cytochrome *c* to $(BChl)_2^+$ was in the opposite direction, and its magnitude was larger (k_D/k_H = 0.7) than that for the isotope effect for electron transfer from Q_A^- to $(BChl)_2^+$ found in this work (k_D/k_H = 1.06). This difference may be explained by a modification of the same simple model that was used for the isotope effect described in this work (see Fig. 5*b*). The cytochrome reaction shows a significant temperature dependence, indicating a thermally activated process. The transition state in this case is not at the minimum of the potential energy curve (i.e., not at the center of the probability distribution) as was the case in the activationless process. Instead, the transition state occurs some distance away from the potential energy minimum in the wings of the probability distribution. Since deuteration causes a decrease in the width of the probability distribution, the probability density near the transition state is lowered, giving rise to a slower electron-transfer rate, in agreement with the experimental observation.

In summary, our work shows a small but significant isotope effect due to slowly exchangeable protons. This indicates that the hydrogen-bonding protons associated with Q_A provide a vibrational mode that is important in the electron-transfer reaction. Other hydrogen-bond modes may assist in vibronic coupling to other electron-transfer events in the RC. For instance, in addition to Q_A and Q_B, both the BChl dimer and the BPh acceptor in the *R. viridis* RC are hydrogen-bonded to protein residues (33). A more detailed description of the role of hydrogen-bonding vibrational modes on the different electron-transfer reactions in the RC remains to be determined.

We thank Ed Abresch for preparing the reaction centers, R. A. Isaacson for his help in the ENDOR experiments, and D. Fredkin and W. Lubitz for helpful discussions. This work was supported by the National Science Foundation Grant PCM 82-02811.

1. Okamura, M. Y., Feher, G. & Nelson, N. (1982) in *Photosynthesis: Energy Conversion by Plants and Bacteria*, ed. Govindjee (Academic, New York), Vol. 1, pp. 195–272.
2. Parson, W. W. & Ke, B. (1982) in *Photosynthesis: Energy Conversion by Plants and Bacteria*, ed. Govindjee (Academic, New York), Vol. 1, pp. 331–385.
3. Michel-Beyerle, M. E., ed. (1985) *Antennas and Reaction Centers of Photosynthetic Bacteria* (Springer Series in Chemical Physics, Springer, Berlin), Vol. 42.
4. Deisenhofer, J., Epp, O., Miki, K., Huber, R. & Michel, H. (1984) *J. Mol. Biol.* **180**, 385–398.
5. Deisenhofer, J., Epp, O., Miki, K., Huber, R. & Michel, H. (1985) *Nature (London)* **318**, 618–624.
6. Williams, J. C., Steiner, L. A., Ogden, R. C., Simon, M. I. & Feher, G. (1983) *Proc. Natl. Acad. Sci. USA* **80**, 6505–6509.
7. Williams, J. C., Steiner, L. A., Feher, G. & Simon, M. I. (1984) *Proc. Natl. Acad. Sci. USA* **81**, 7303–7307.
8. Michel, H., Weyer, K. A., Gruenberg, H., Dunger, I., Oesterhelt, D. & Lottspeich, F. (1986) *EMBO J.* **5**, 1149–1158.
9. Allen, J. P., Feher, G., Yeates, T. O., Rees, D. C., Eisenberg, D. S., Deisenhofer, J., Michel, H. & Huber, R. (1986) *Biophys. J.* **49**, 583 (abstr.).
10. Marcus, R. A. (1964) *Annu. Rev. Phys. Chem.* **15**, 155–196.
11. Hopfield, J. J. (1974) *Proc. Natl. Acad. Sci. USA* **71**, 3640–3644.
12. Jortner, J. (1976) *J. Chem. Phys.* **64**, 4860–4867.
13. Kakitani, T. & Kakitani, H. (1981) *Biochim. Biophys. Acta* **635**, 498–514.
14. Sarai, A. (1980) *Biochim. Biophys. Acta* **589**, 71–83.
15. Lubitz, W., Abresch, E. C., Debus, R. J., Isaacson, R. A., Okamura, M. Y. & Feher, G. (1985) *Biochim. Biophys. Acta* **808**, 464–469.
16. Feher, G., Isaacson, R. A., Okamura, M. Y. & Lubitz, W. (1985) in *Antennas and Reaction Centers of Photosynthetic Bacteria*, ed. Michel-Beyerle, M. E. (Springer Series in Chemical Physics, Springer, Berlin), Vol. 42, pp. 174–189.
17. Debus, R. J., Feher, G. & Okamura, M. Y. (1986) *Biochemistry* **25**, 2276–2287.
18. Blankenship, R. E. & Parson, W. W. (1979) *Photosynthesis in Relation to Model Systems*, ed. Barber, J. (Elsevier, New York), pp. 71–114.
19. Feher, G., Okamura, M. Y. & Kleinfeld, P. (1986) *Conference on Protein-Structure: Molecular and Electronic Reactants* (Springer, Berlin), in press.
20. Gunner, M. R., Robertson, D. E. & Dutton, P. L. (1986) *J. Phys. Chem.*, in press.
21. Parson, W. W. (1967) *Biochim. Biophys. Acta* **131**, 154–172.
22. Clayton, R. K. & Yau, H. F. (1972) *Biophys. J.* **12**, 867–881.
23. Hsi, E. S. P. & Bolton, J. R. (1974) *Biochim. Biophys. Acta* **347**, 126–133.
24. McElroy, J. D., Mauzerall, D. C. & Feher, G. (1974) *Biochim. Biophys. Acta* **333**, 261–278.
25. Loach, P. A., Kung, M. C. & Hales, J. B. (1975) *Ann. N.Y. Acad. Sci.* **244**, 297–319.
26. Hopfield, J. J. (1976) in *Electrical Phenomena at the Biological Membrane Level*, ed. Roux, E. (Elsevier, Amsterdam), pp. 471–492.
27. Jortner, J. J. (1980) *J. Am. Chem. Soc.* **102**, 6676–6686.
28. Okamura, M. Y. & Feher, G. (1986) *Biophys. J.* **49**, 587 (abstr.).
29. Feher, G. & Okamura, M. Y. (1978) in *The Photosynthetic Bacteria*, eds. Clayton, R. K. & Sistrom, W. R. (Plenum, New York), pp. 349–386.
30. Okamura, M. Y., Isaacson, R. A. & Feher, G. (1975) *Proc. Natl. Acad. Sci. USA* **72**, 3491–3495.
31. Kleinfeld, D., Okamura, M. Y. & Feher, G. (1984) *Biochim. Biophys. Acta* **766**, 126–140.
32. Kihara, T. & McCray, J. A. (1973) *Biochim. Biophys. Acta* **292**, 297–309.
33. Michel, H., Epp, O. & Deisenhofer, J. (1986) *EMBO J.* **5**, 2445–2451.